

Supplementary Material

Decoding optimal ligand design for multicomponent condensates

Sarasi K. K. Galagedera¹, Thuy P. Dao¹, Suzanne E. Enos¹, Antara Chaudhuri¹,
Jeremy D. Schmit^{2,*}, and Carlos A. Castañeda^{1,3,4,*}

Table of Contents

Theory for Ligand-mediated phase transitions

Figure S1

Figure S2

Figure S3

Figure S4

Figure S5

Figure S6

Figure S7

Figure S8

Figure S9

Figure S10

Figure S11

Table S1

Table S2

Table S3

Table S4

Table S5

Theory for ligand-mediated phase transitions

Solution Free Energy

We have developed a theory to reconcile the observation that monoubiquitin and polyubiquitin inhibit and promote phase separation respectively. The first requirement of the model is that it must capture the binding equilibrium of ubiquitin and UBQLN2 into higher order complexes. We begin by writing down the free energy of the dilute state, which we denote with the index V = "vapor":

$$F_V = c_{h,V} \left(\ln \frac{c_{h,V}}{c_0} - 1 + f_h \right) + c_{d,V} \left(\ln \frac{c_{d,V}}{c_0} - 1 + f_d \right) + \sum_{n=1}^N c_{n,V} \left(\ln \frac{c_{n,V}}{c_0} - 1 + f_n \right) + \mu_h (c_{H,V} - c_{h,V} - \sum_{n=1}^N c_{n,V}) + \mu_d (c_{D,V} - c_{d,V} - \sum_{n=1}^N n c_{n,V}) \quad (\text{Eq. S1})$$

Here $c_{h,V}$ and $c_{d,V}$ are the concentrations of hub and driver molecules in the monomer state, respectively (i.e., not bound to any other hub or driver molecule). N is the number of driver molecules that a hub can bind (N=4 in the case of Ub4) and $c_{n,V}$ is the concentration of hubs that are bound to n driver molecules ("n-mers"). f_i is the free energy of species i and $c_i \left(\ln \frac{c_i}{c_0} - 1 \right)$ is the mixing entropy of that species, where c_0 is a reference concentration. The chemical potentials μ_h and μ_d serve as Lagrange multipliers to ensure that the concentration of molecules in the monomer and n-mer states add up to the total concentration of hubs, $c_{H,i}$, and driver molecules, $c_{D,i}$. (In our notation, the capital index (e.g. H, D) indicates the total concentration while the lowercase (e.g. h, d) indicates the monomer state).

The free energy of the dense state (denoted with the subscript L = "liquid") has a similar form:

$$F_L = c_{h,L} \left(\ln \frac{c_{h,L}}{c_0} - 1 + f_h + s_h \right) + c_{d,L} \left(\ln \frac{c_{d,L}}{c_0} - 1 + f_d + s_d \right) + \sum_{n=1}^N c_{n,L} \left(\ln \frac{c_{n,L}}{c_0} - 1 + f_n + s_n \right) + \mu_h (c_{H,L} - c_{h,L} - \sum_{n=1}^N c_{n,L}) + \mu_d (c_{D,L} - c_{d,L} - \sum_{n=1}^N n c_{n,L}) \quad (\text{Eq. S2})$$

Where s_i is the energy to transfer species i from the dilute, vapor (V) state to the liquid (L) state (e.g. s_h is the energy to transfer the hub from the vapor to liquid state).

Chemical and Partitioning Equilibrium

Minimizing F_V and F_L with respect to c_i we find expressions for each of the species concentrations in the vapor phase:

(Eq. S3)

$$\begin{aligned}
c_{h,V} &= c_0 e^{-f_h + \mu_h} \\
c_{d,V} &= c_0 e^{-f_d + \mu_d} \\
c_{n,V} &= c_0 e^{-f_n + \mu_h + n\mu_d}
\end{aligned}$$

And in the liquid phase:

(Eq. S4)

$$\begin{aligned}
c_{h,L} &= c_0 e^{-f_h - s_h + \mu_h} \\
c_{d,L} &= c_0 e^{-f_d - s_d + \mu_d} \\
c_{n,L} &= c_0 e^{-f_n - s_n + \mu_h + n\mu_d}
\end{aligned}$$

The expressions for the monomers in the vapor phase can be rearranged to find expressions for the chemical potentials:

(Eq. S5)

$$\begin{aligned}
\mu_h &= \ln \frac{c_{h,V}}{c_0} + f_h \\
\mu_d &= \ln \frac{c_{d,V}}{c_0} + f_d
\end{aligned}$$

These expressions can be used with Eqs. S3 and S4 to obtain the conditions for (unbound) monomer phase partitioning:

(Eq. S6)

$$\begin{aligned}
c_{h,V} &= c_{h,L} e^{s_h} \\
c_{d,V} &= c_{d,L} e^{s_d}
\end{aligned}$$

Similarly, the chemical potentials can be substituted in the expressions for the n-mer concentrations:

(Eq. S7)

$$\begin{aligned}
c_{n,V} &= \frac{c_{h,V} c_{d,V}^n}{c_0^n} e^{-(f_n - f_h - n f_d)} \\
&= \frac{c_{h,V} c_{d,V}^n}{k_{n,V}}
\end{aligned}$$

Where $k_{n,V}$ is the dissociation constant for the formation of n-mers in the dilute (vapor) phase.

Similarly, in the dense (liquid) phase we find:

(Eq. S8)

$$\begin{aligned}
c_{n,L} &= \frac{c_{h,L} c_{d,L}^n}{c_0^n} e^{-(f_n - f_h - n f_d) - (s_n - s_h - n s_d)} \\
&= \frac{c_{h,L} c_{d,L}^n}{k_{n,L}}
\end{aligned}$$

where

(Eq. S9)

$$k_{n,L} = k_{n,V} e^{(s_n - s_h - ns_d)}$$

$$k_{n,L} = k_{n,V} e^{\Delta s}$$

Note that if the transfer free energy of an n-mer is given by the sum of its parts such that $s_n = s_h + ns_d$ then the dissociation constants are identical in each phase. Therefore, Δs , is a parameter that describes how oligomerization (hub-driver binding) modifies the interaction with the fluid (driver-only fluid). However, if the bonding constraints within the n-mer perturb the interactions with the surrounding phase, the oligomerization equilibrium will be different between the phases (Δs will be non-zero).

The above formulation ensures that binding equilibria are satisfied in each phase and that the chemical potentials for each species are equal across phases.

Our next task is to determine a condition for the onset of phase separation. At the onset, we can consider the dense phase to be infinitesimally small so that all of the proteins are in the dilute (vapor) phase. Thus, $c_{H,V}$ and $c_{D,V}$ are equal to the total protein concentrations, which can be used with Eq. S7 to determine the monomer concentration ($c_{h,V}$ and $c_{d,V}$ (as described below)). These concentrations, in turn, can be used with Eq. S8 to find the monomer concentrations in the infinitesimal droplet. Next these concentrations are used with Eq. S9 to find the concentration of n-mers in the dense phase.

Saturated Solution Condition

To assess whether these concentrations represent a subsaturated or supersaturated solution we examine the total concentration of the driver molecules in the dense phase. When polymers phase separate, the mass concentration of the dense phase is insensitive to the molecular weight (or equivalently the polymerization number) of the individual molecules (57). This is because the microscopic interactions and mesh structure of the phase are both much smaller than the molecules. In agreement with this expectation, the concentration of UBQLN2 molecules in the dense phase is nearly constant regardless of whether the UBQLN2 are monomers or oligomerized by a hub (8). Therefore, we adopt, as the criteria for phase separation, the condition that the total concentration of UBQLN2 in the dense phase is equal to the concentration of the UBQLN2-only fluid (i.e. in a UBQLN2-only phase separating solution):

$$c_{d,L} + \sum_n n c_{n,L} = c_{D,L} \quad (\text{Eq. S10})$$

where the total concentration $c_{D,L}$ is taken to be the constants $c_{D,L} = 10$ mM for 450C and $c_{D,L} = 2$ mM for full length UBQLN2 (8).

An important insight from Eq. S10 is that hub molecules facilitate phase separation by lowering the chemical potential of driver molecules in the dense phase. This is most easily seen by examining the unbound driver chemical potentials in the two limiting cases:

- In a sub-saturated solution, the UBQLN2 concentration will add up to less than the pure UBQLN2 fluid: $c_{d,L} + \sum_n n c_{n,L} < c_{D,L}$. In this case, the dense phase will collapse to fill the voids and optimize the UBQLN2-UBQLN2 contacts. After this collapse, the monomer (unbound driver) concentration in the dense phase will increase such that the chemical potential in the dense phase is greater than the dilute phase: $\ln \frac{c_{d,V}}{c_0} < \ln \frac{c_{d,L}}{c_0} + s_d$. This will drive the monomers (unbound drivers) to leave the dense phase, causing it to shrink.
- Conversely, in a supersaturated solution we would find $c_{d,L} + \sum_n n c_{n,L} > c_{D,L}$ implying that the driver molecules are packed too close together. In this case the dense phase will expand, lowering the concentration of monomers. Again comparing the resulting chemical potentials of the monomers we find $\ln \frac{c_{d,V}}{c_0} > \ln \frac{c_{d,L}}{c_0} + s_d$, which will drive additional monomers (unbound complexes) to enter the dense phase.

Therefore, the condition for the onset of phase separation is when Eq. S10 is satisfied and the monomer concentrations satisfy

$$\ln \frac{c_{d,V}}{c_0} = \ln \frac{c_{d,L}}{c_0} + s_d \quad (\text{Eq. S11})$$

Which is equivalent to Eq. S6.

In the absence of hubs ($c_{D,L} = c_{d,L}$), this expression gives Eq. 3 from the main text:

$$\frac{c_{sat}}{c_{D,L}} = e^{s_d} \quad (\text{Eq. S12})$$

Temperature Dependence of Phase Separation

The temperature dependence of s_d is modeled by fitting the experimental cloud point temperatures to the quadratic function:

$$c_{sat} = a(T - T_c)^2 + c_c \quad (\text{Eq. S13})$$

The best fit parameters are shown in Fig. S10. Combining this with our previous result (Eq. S12) we have:

$$e^{s_d} = \frac{c_{sat}}{c_{D,L}} \quad (\text{Eq. S14})$$

$$e^{s_d} = \frac{a(T - T_c)^2 + c_c}{c_{D,L}}$$

Next, we express our condition for phase separation in terms of s_d :

$$c_{D,L} = c_{d,L} + \sum_n n c_{n,L}$$

$$c_{D,L} = c_{d,L} + \sum_n n \frac{c_{h,L} c_{d,L}^n}{k_{n,L}}$$

(Eq. S15)

Using Eqs. S6 and S9 this becomes

$$c_{D,L} = c_{d,V} e^{-s_d} + c_{h,V} e^{-s_h} \sum_n n \frac{(c_{d,V} e^{-s_d})^n}{k_{n,V} e^{\Delta s}}$$

$$1 = \frac{c_{d,V}}{c_{sat}} + \frac{c_{h,V} e^{-s_h}}{c_{D,L}} \sum_n n \frac{\left(\frac{c_{d,V} c_{D,L}}{c_{sat}}\right)^n}{k_{n,V} e^{\Delta s}}$$

(Eq. S16)

Finally, to reduce the number of free parameters in the model, we make the approximation that Δs is independent of n and obtain:

$$1 = \frac{c_{d,V}}{c_{sat}} + \frac{c_{h,V} e^{-s_h - \Delta s}}{c_{D,L}} \sum_n n \frac{\left(\frac{c_{d,V} c_{D,L}}{c_{sat}}\right)^n}{k_{n,V}}$$

(Eq. S17)

We refer to the quantity $s_h + \Delta s$ as the “inclusion energy”. It accounts for two detrimental effects from transferring an n -mer to the dense phase. The first is the repulsive solvation energy of the hub and the second is the constraints preventing the bound drivers from attaining their optimal interactions with the fluid. This inclusion energy is the only free parameter in Eq. S17.

Calculation of Cloud Point Curves

Comparison between theory and experiment is complicated by the fact that Eq. S17 depends on the monomer (unbound) concentrations c_d and c_h , which are not readily known from experiments. These quantities can be determined from the total concentrations as follows. First, we construct the partition function of a hub in the vapor phase:

$$Q_h = 1 + \sum_{n=1}^N \frac{c_d^n}{k_{n,V}}$$

(Eq. S18)

Where we approximate the equilibrium constants by assuming independent sites such that $k_{n,V} = k_0^n / n!$, where k_0 is the dissociation constant between monoubiquitin and UBQLN2 at

25°C (Table S1) and $\binom{N}{n}C$ is a binomial coefficient accounting for the multiplicity of binding. From the partition function we obtain an expression for the average number of bound drivers per hub

$$\langle n \rangle = \frac{1}{Q_h} \sum_{n=1}^N n \frac{c_d^n}{k_{n,V}} \quad (\text{Eq. S19})$$

With this expression we can write an equation for c_d in terms of the total concentrations:

$$c_D = c_d + \langle n \rangle c_H \quad (\text{Eq. S20})$$

The left side of c_d monotonically increases for positive values of c_d , meaning that there is only one root within the range $0 < c_d \leq c_D$ that can be readily found numerically. With c_d known, c_h is obtained from the statistical weight of the monomer term in the partition function

$$c_h = \frac{c_H}{Q_h} \quad (\text{Eq. S21})$$

The quantities c_h and c_d are inserted into Eq. S17, along with Eq. S13, which is numerically solved for the onset temperature.

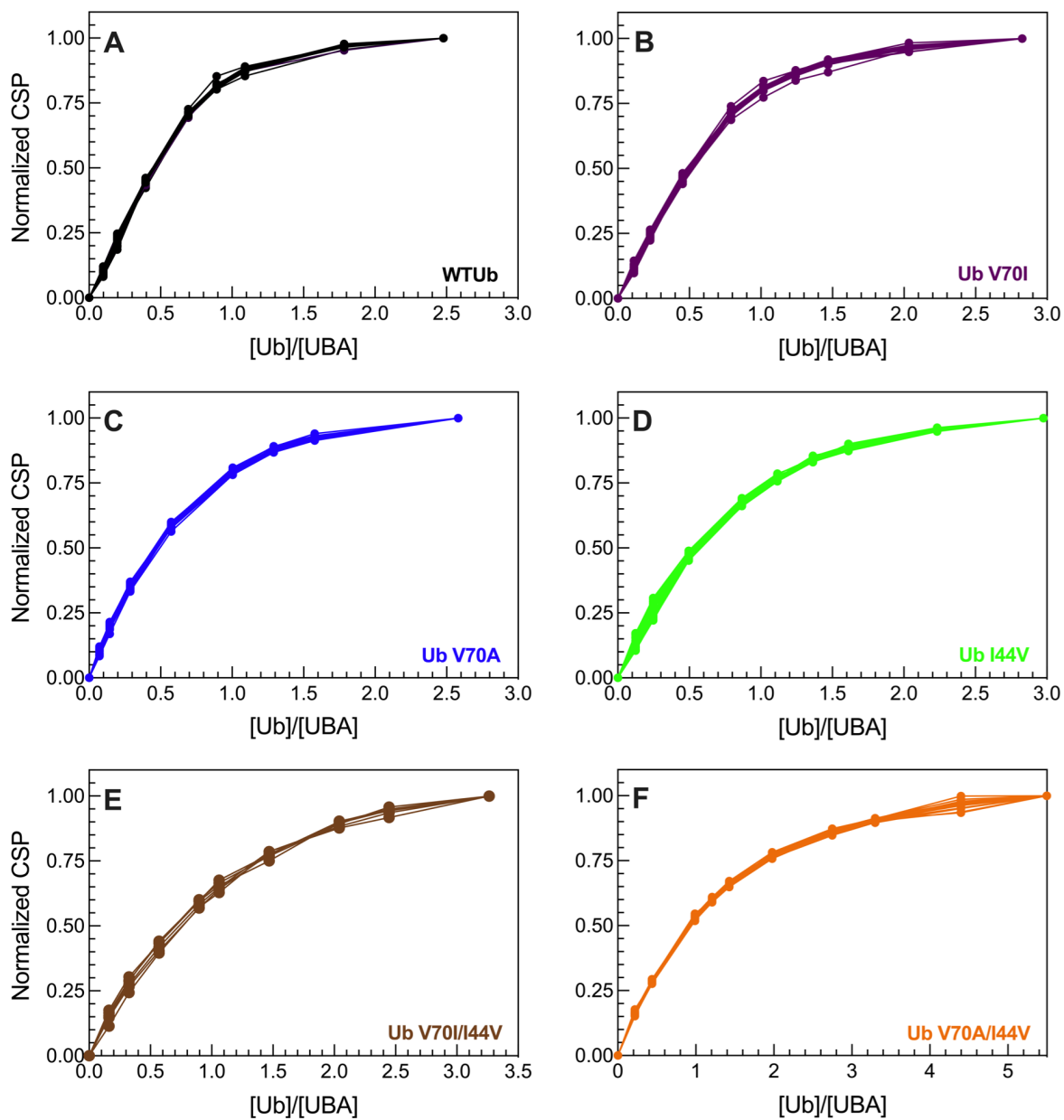


Figure S1. Residue-specific normalized backbone amide titration curves for 100 μM ^{15}N UBQLN2 UBA resonances after titrating 0-250 μM of (A) WT Ub [22 amino acid resonances], (B) Ub V70I [21], (C) Ub V70A [17], (D) Ub I44V [23], (E) Ub V70I/I44V [6], & (F) Ub V70A/I44V [18]. See Table S1 for a list of specific amino acid resonances used.

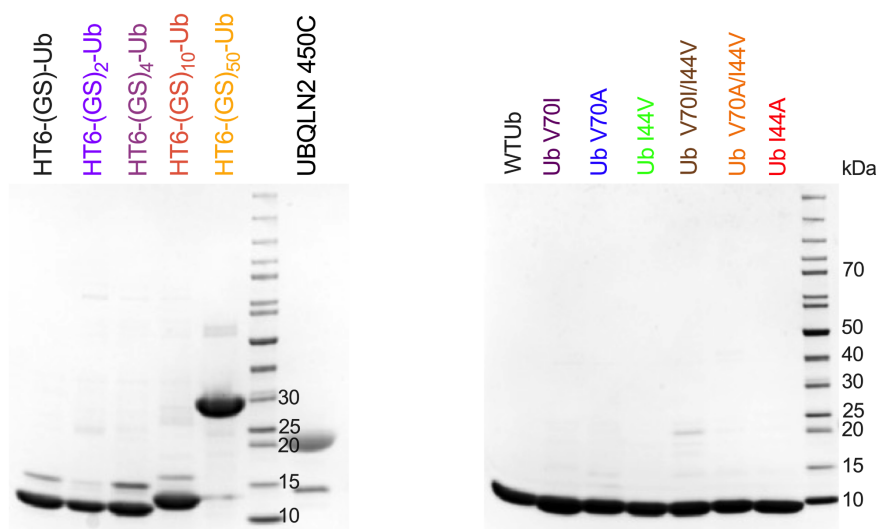


Figure S2. Representative Mini-PROTEAN TGX Precast gel images of (A) HT6-Ub and UBQLN2 450C, and (B) Ub mutants used in this study.

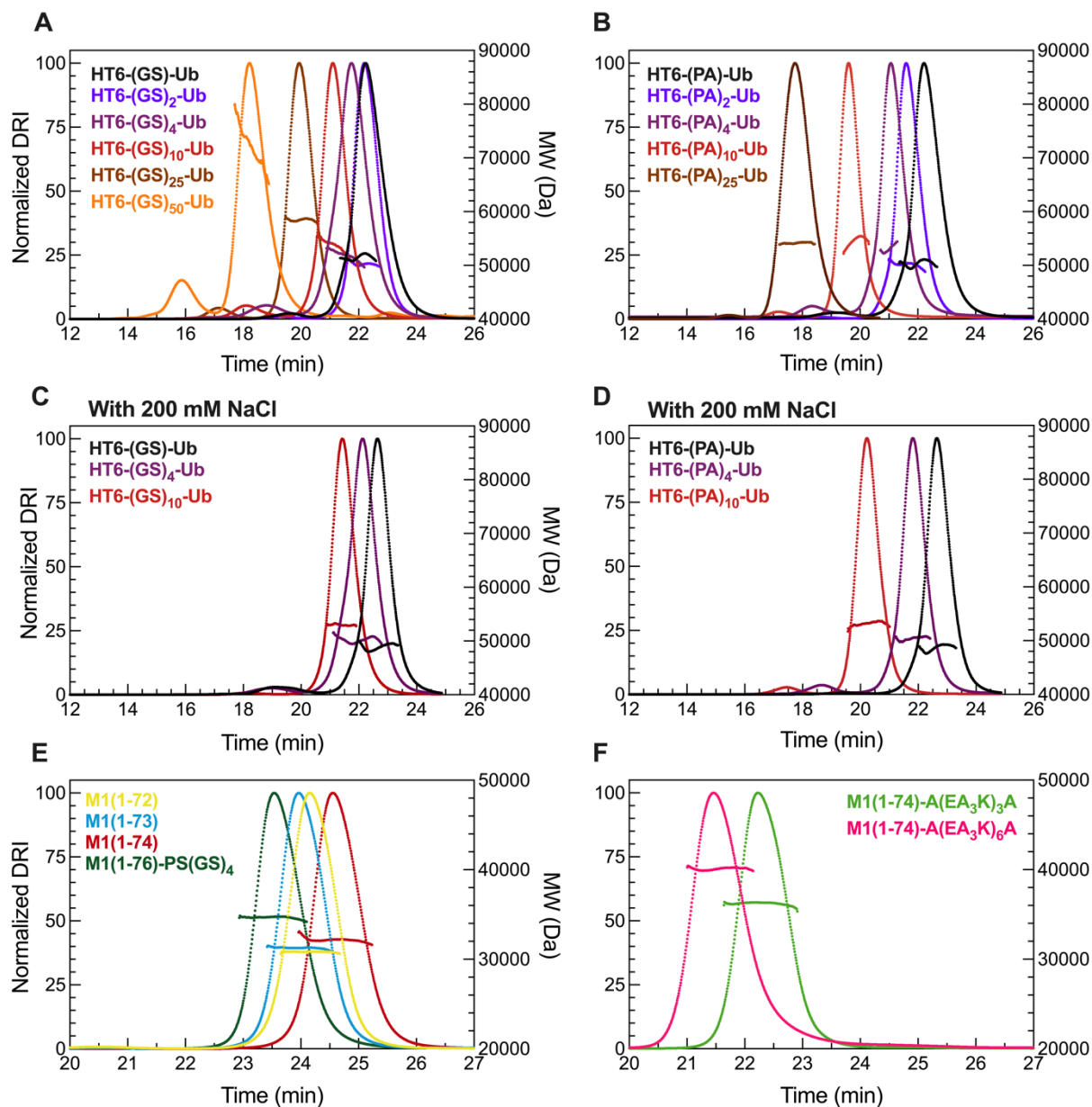


Figure S3. SEC-MALS profiles for various Ub₄ ligand hubs used in this study. As expected, HT6-Ub is a tetramer. The molecular weight (MW) of (A) HT6-(GS)_x-Ub (B) HT6-(PA)_x-Ub (E) M1-linked Ub₄ chains, and (F) M1-linked Ub₄ chains with long Ub-Ub linkers were determined using SEC-MALS experiments. To test for the effect of salt on HT6-Ub oligomerization, we collected represented SEC-MALS profiles for (C) HT6-(GS)_x-Ub and (D) HT6-(PA)_x-Ub hubs. For all profiles collected above, the observed MW values are consistent with the expected MW of these constructs.

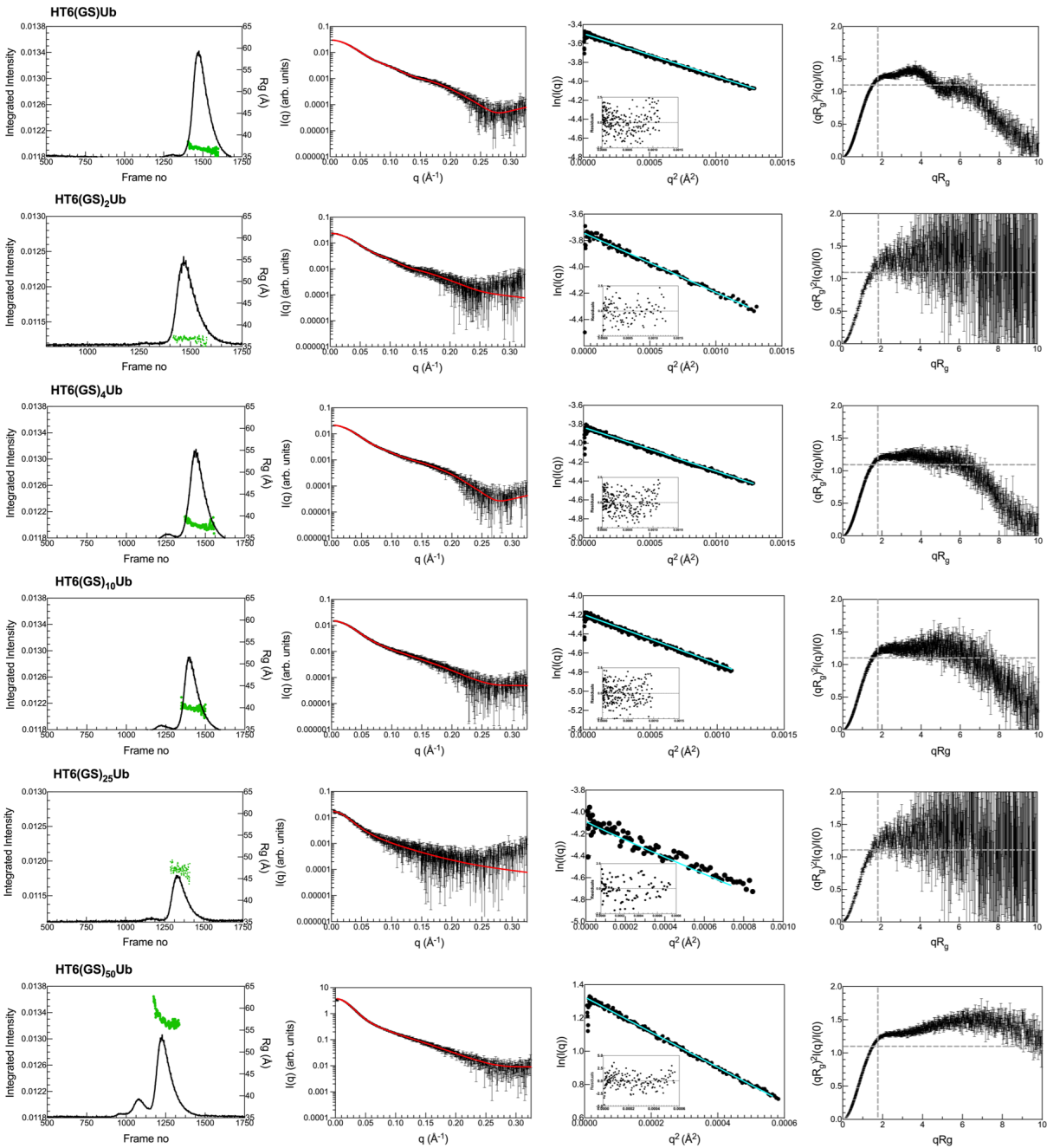


Figure S4A. (Left) SEC-SAXS profiles for HT6-(GS)-Ub, HT6-(GS)₄-Ub, HT6-(GS)₁₀-Ub, & HT6-(GS)₅₀-Ub. $I(q)$ vs. q scattering curves (middle left) determined from frames (1438-1475) HT6-(GS)-Ub, (1453-1465) HT6-(GS)₂-Ub, (1448-1500) HT6-(GS)₄-Ub, (1423-1469) HT6-(GS)₁₀-Ub, (1322-1325) HT6-(GS)₂₅-Ub & (1165-1399) HT6-(GS)₅₀-Ub on the corresponding SEC-SAXS profiles (left). Red line in the $I(q)$ profile indicates fit from $P(r)$ analysis (see Fig. 2C). Cyan line in the Guinier plot (middle right) is the linear fit of $\ln(I(q))$ vs. q^2 , while inset shows residuals of fit. Dimensionless Kratky plots (right) include dashed lines to indicate where a globular protein would peak. Increase in polyUb chain flexibility from top (HT6-(GS)-Ub) to bottom (HT6-(GS)₅₀-

Ub) is indicated by shifts in the peak position up and to the right of the globular peak and larger plateaus in the higher q region.

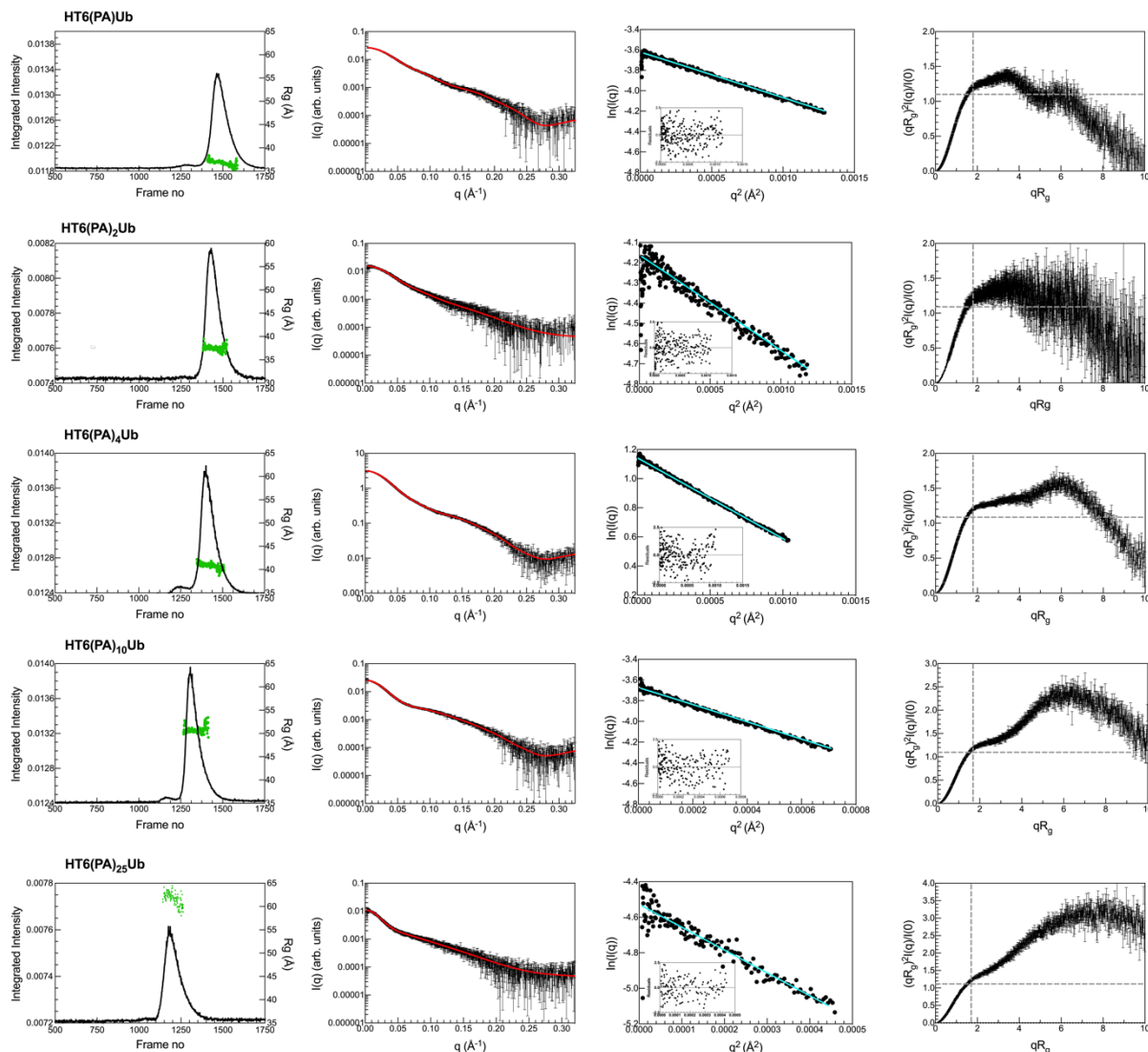


Figure S4B. SEC-SAXS profiles for HT6-(PA)-Ub, HT6-(PA)₂-Ub, HT6-(PA)₄-Ub, HT6-(PA)₁₀-Ub & HT6-(PA)₂₅-Ub. $I(q)$ vs. q scattering curves (middle left) determined from frames (1478-1502) HT6-(PA)-Ub, (1425-1430) HT6-(PA)₂-Ub, (1452-1476) HT6-(PA)₄-Ub, (1352-1376) HT6-(PA)₁₀-Ub & (1183-1195) HT6-(PA)₂₅-Ub on the corresponding SEC-SAXS profiles (left). Red line in the $I(q)$ profile indicates fit from $P(r)$ analysis (see Fig. 2C). Cyan line in the Guinier plot (middle right) is linear fit of $\ln(I(q))$ vs. q^2 , while inset shows residuals of fit. Dimensionless Kratky plots (right) include dashed lines to indicate where a globular protein would peak. Increase in polyUb chain flexibility from top (HT6-(PA)-Ub) to bottom (HT6-(PA)₂₅-Ub) is indicated by shifts in the peak position up and to the right of the globular peak and larger plateaus in the higher q region.

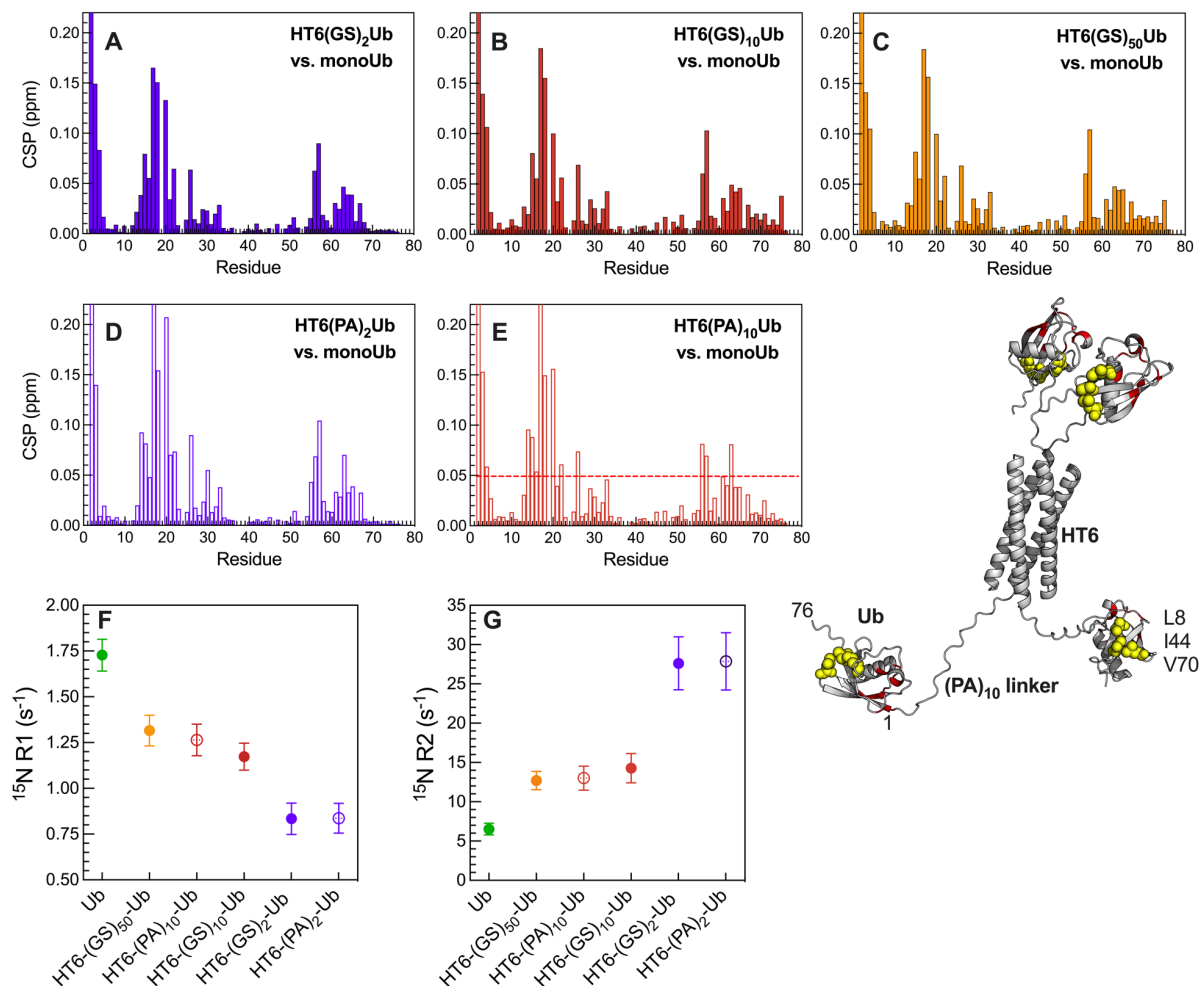


Figure S5. Comparison of Ub amide chemical shift perturbations (CSPs) for resonances in (A) HT6-(GS)₂-Ub, (B) HT6-(GS)₁₀-Ub, (C) HT6-(GS)₅₀-Ub, (D) HT6-(PA)₂-Ub, (E) HT6-(PA)₁₀-Ub vs. monoUb. CSPs > 0.05 ppm for (E) were mapped onto representative HT6-(PA)₁₀-Ub structure (see Fig. 2B) showing that only resonances spatially near the linker were perturbed, while not impacting the hydrophobic patch of Ub (yellow spheres). (F, G) Average ¹⁵N R₁ and R₂ relaxation rates for Ub resonances in secondary structure organized in terms of decreasing R₁ and increasing R₂ rates. Error bars denote standard deviation of residue-specific relaxation rates (>63 residues used) per construct.

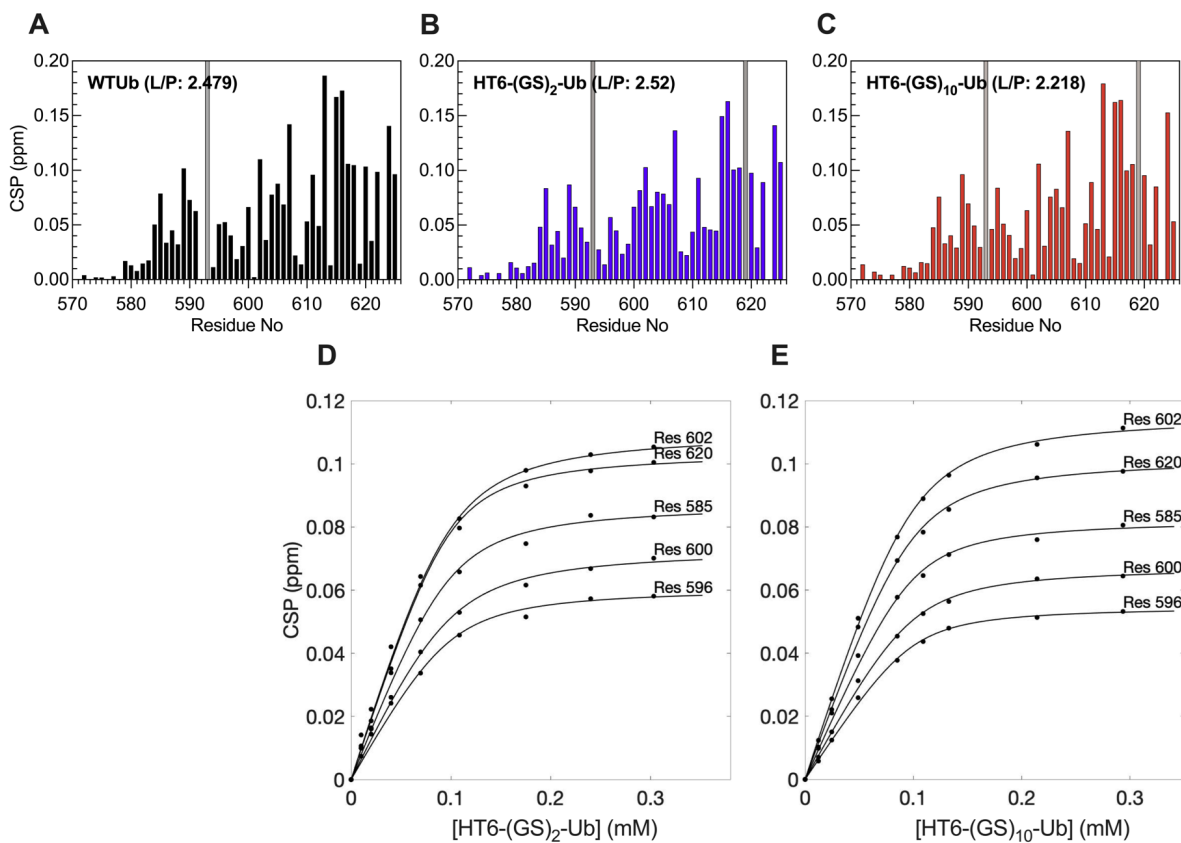


Figure S6. Comparison of backbone amide CSPs for UBA UBQLN2 (100 μ M) upon titration with (A) WT Ub (ligand:protein (L:P)=2.48), (B) HT6-GS₂-Ub (L:P=2.52) & (C) HT6-GS₁₀-Ub (L:P=2.22). Gray bars mark the resonances that are completely attenuated at the end of the titration. (D,E) Residue-specific amide titration curves of (D) HT6-(GS)₂-Ub, and (E) HT6-(GS)₁₀-Ub. Here fits from a single-site binding model were superpositioned on experimental data points.

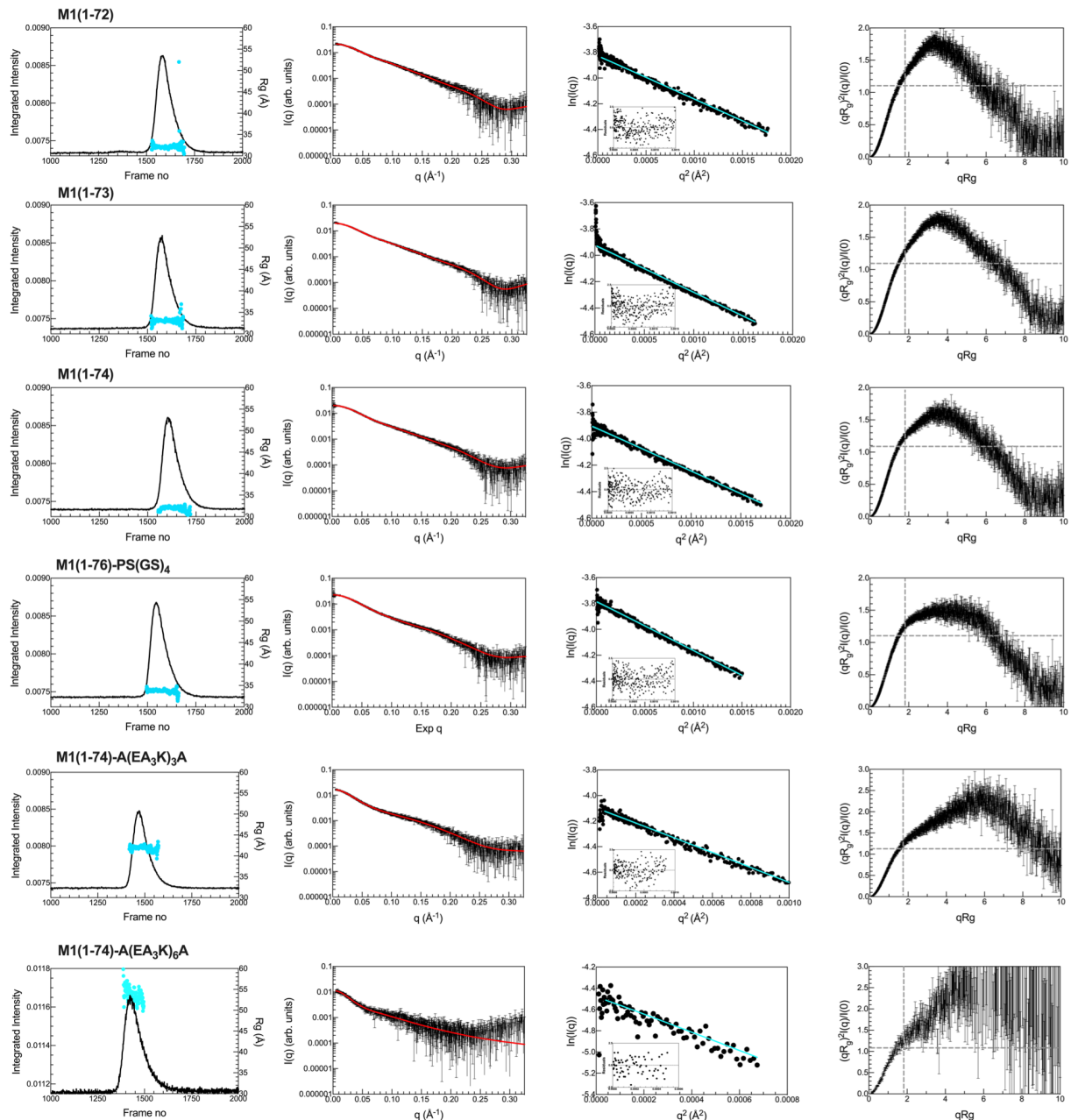


Figure S7. SEC-SAXS profiles for M1(1-72), M1(1-73), M1(1-74), M1(1-76)-PS(GS)₄, M1(1-74)-A(EA₃K)₃A & M1(1-74)-A(EA₃K)₆A. $I(q)$ vs. q scattering curves (middle left) determined from frames (1580-1586) M1(1-72), (1556-1577) M1(1-73), (1592-1605) M1(1-74), (1540-1551) M1(1-76)-PS(GS)₄, (1440-1450) M1(1-74)-A(EA₃K)₃A, & (1437-1440) M1(1-74)-A(EA₃K)₆A on the corresponding SEC-SAXS profiles (left). Red line in the $I(q)$ profile indicates fit from $P(r)$ analysis (see Fig. 4). Cyan line in the Guinier plot (middle right) is linear fit of $\ln(I(q))$ vs. q^2 , while inset shows residuals of fit. Dimensionless Kratky plots (right) include dashed lines to indicate where a globular protein would peak.

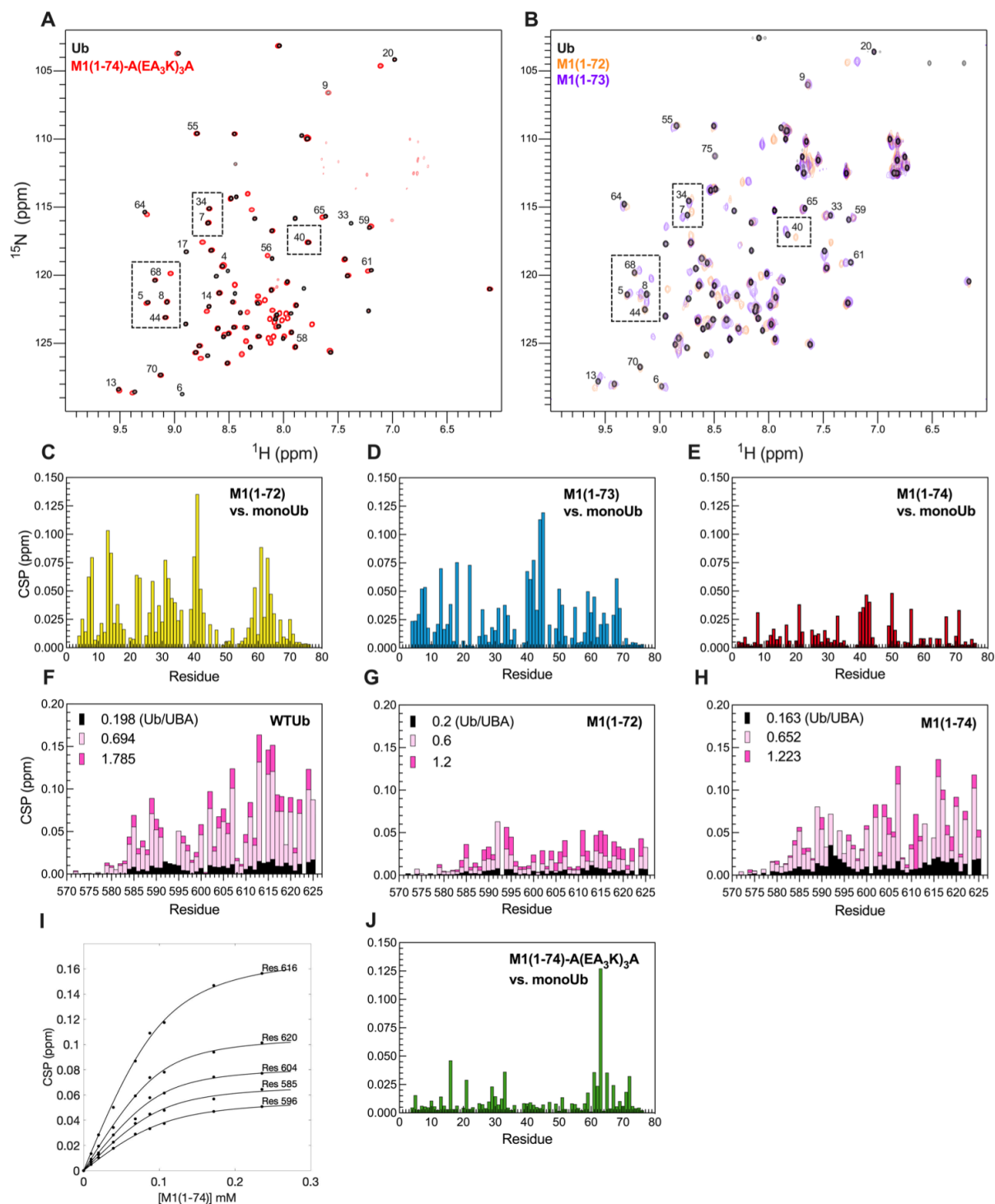


Figure S8. (A) ^{15}N - ^1H TROSY-HSQC spectra of 200 μM ^{15}N labeled Ub (black) and M1-Ub4 (1-74)-A(EA₃K)₃A (red). (B) ^{15}N - ^1H SOFAST-HMQC spectra of 100 μM ^{15}N labeled Ub (black), 200 μM M1-Ub4 (1-72) (orange), and 200 μM M1-Ub4 (1-73) (purple). Natural abundance spectra for M1-Ub4 (1-72) and M1-Ub4 (1-73) were collected with >1024 scans. Spectra were collected at 25 °C in 20 mM NaPhosphate buffer pH 6.8. (C, D, E) Chemical shift perturbations (CSPs) measured for backbone amide resonances in (C) M1-Ub4 (1-72), (D) M1-Ub4 (1-73), (E) M1-

Ub4 (1-74) with respect to ^{15}N labeled monoUb resonances under identical buffer conditions. (F, G, H) Amide CSPs measured at three different Ub: ^{15}N UBA ratios (as noted in figure) upon titrating unlabeled (F) WT Ub (G) M1-Ub4 (1-72) (H) M1-Ub4 (1-74) into $100\ \mu\text{M}$ ^{15}N UBA UBQLN2. (I) Residue-specific backbone amide titration curves for UBA resonances as unlabeled M1-Ub4 (1-74) was titrated into $100\ \mu\text{M}$ ^{15}N UBA UBQLN2. Single-site binding model (black line) was fit to residue-specific titration curves (data points) to obtain K_d values. (J) Chemical shift perturbations (CSPs) measured for backbone amide resonances in M1(1-74)-A(EA₃K)₃A with respect to ^{15}N labeled monoUb resonances under identical buffer conditions. As we observed multiple resonances for select Ub residues in M1(1-72), M1(1-73), M1(1-74) & M1(1-74)-A(EA₃K)₃A, the largest CSP values for each residue are reported here.

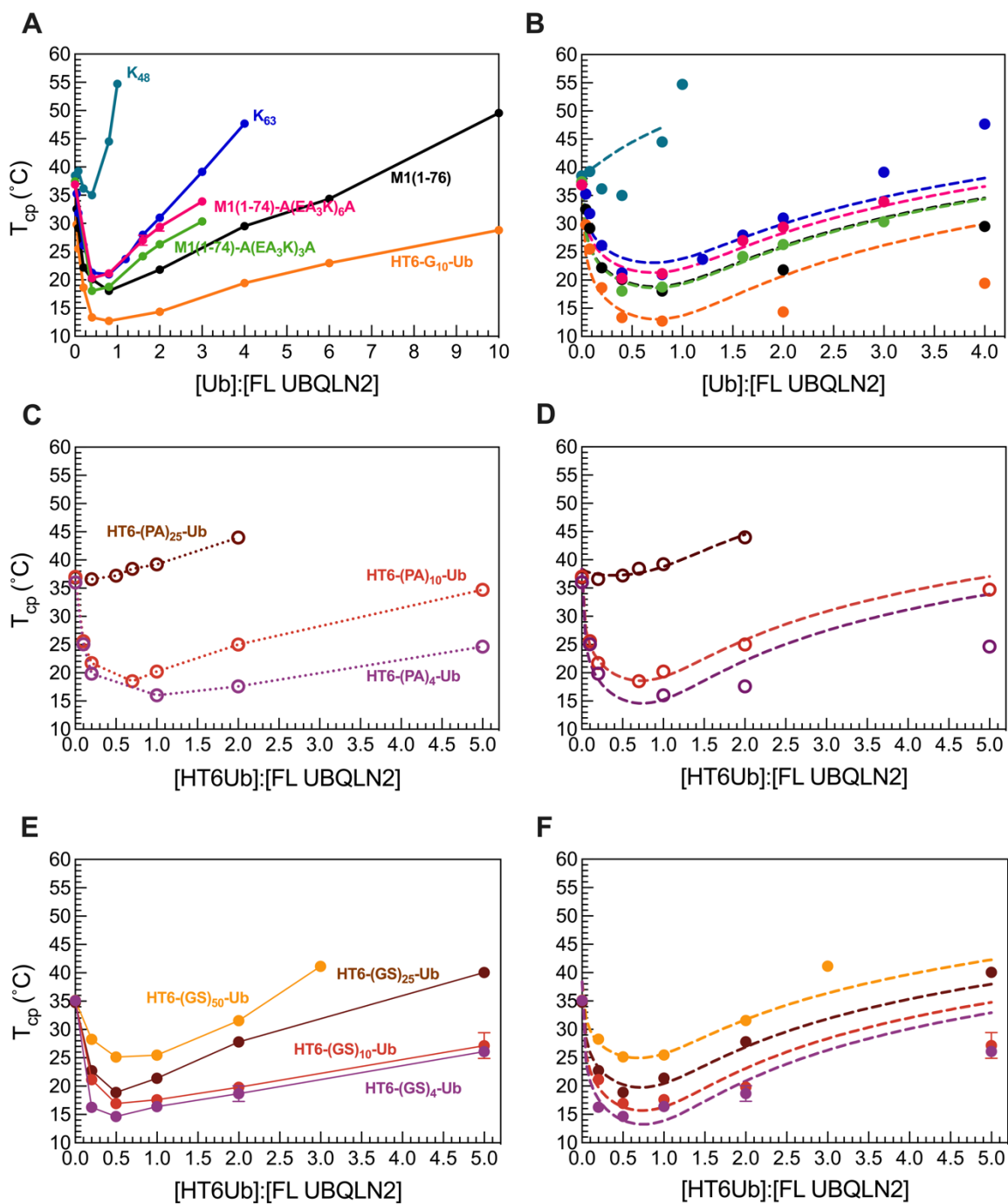


Figure S9. There is an optimal ligand architecture of polyUb that maximizes full-length (FL) UBQLN2 phase separation. (A, C) Experimental phase diagrams of FL UBQLN2 with natural and designed polyUb chains of different linkages. FL UBQLN2 concentration was kept constant at 30 μ M. (B, D) Analytical theory fitted to experimental data.

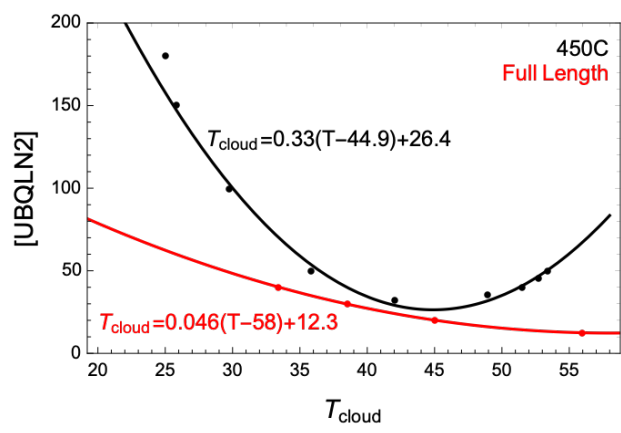


Figure S10. Comparison of experimental cloud point measurements (points) and fits to Eq. S13 for full length UBQLN2 (red) and 450C variant of UBQLN2 (black). Data for full length UBQLN2 and 450C variant of UBQLN2 are from (8) and (58), respectively.

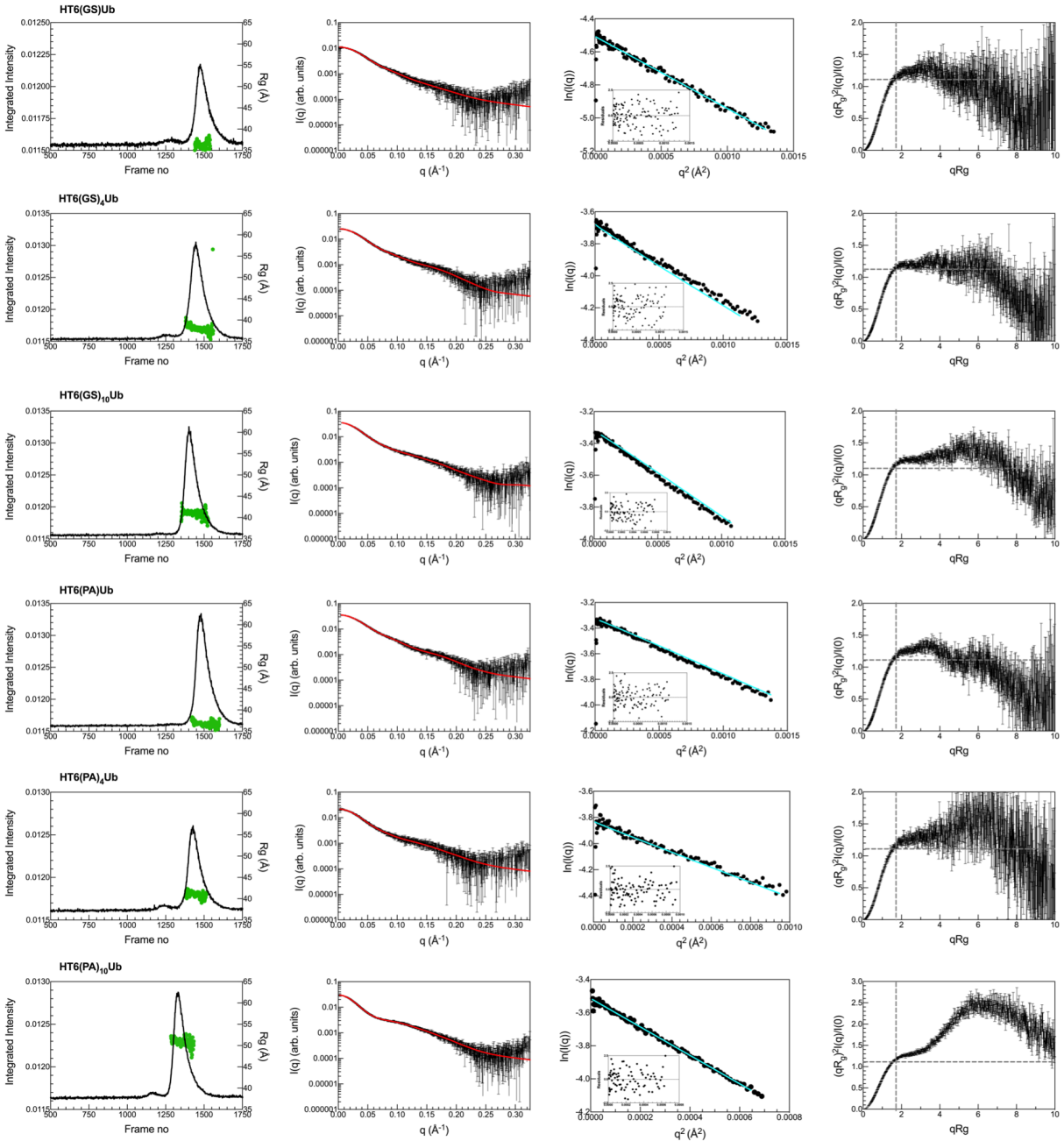


Figure S11. (A) SEC-SAXS profiles for HT6-(GS)-Ub, HT6-(GS)₄-Ub, HT6-(GS)₁₀-Ub, HT6-(PA)-Ub, HT6-(PA)₄-Ub, & HT6-(PA)₁₀-Ub collected in 20 mM phosphate buffer pH 6.8 with 200 mM NaCl, 0.5 mM EDTA & 0.02 % NaAz. $I(q)$ vs. q scattering curves (middle left) determined from frames (1455-1513) HT6-(GS)-Ub, (1459-1482) HT6-(GS)₄-Ub, (1387-1408) HT6-(GS)₁₀-Ub, (1473-1484) HT6-(PA)-Ub, (1418-1428) HT6-(PA)₄-Ub & (1314-1354) HT6-(PA)₁₀-Ub on the corresponding SEC-SAXS profiles (left). Red line in the $I(q)$ profile indicates fit from $P(r)$ analysis. Cyan line in the Guinier plot (middle right) is the linear fit of $\ln(I(q))$ vs. q^2 , while inset shows residuals of fit. Dimensionless Kratky plots (right) include dashed lines to indicate where a globular protein would peak.

Table S1. Calculated average binding affinity (K_d) values of UBQLN2 UBA domain with WT Ub, Ub mutants, HT6-(GS)₂/(GS)₁₀-Ub and M1(1-74) used in the study. The errors represent the standard deviation of K_d values determined from multiple NMR resonances as listed below (see Fig. S1).

Protein	K_d (μ M)	Amino acid resonances used in K_d determination
WT Ub	2.6 ± 0.3	584, 585, 589, 590, 591, 596, 600, 602, 604, 605, 606, 607, 610, 611, 613, 615, 616, 617, 618, 620, 622, 624
V70I	6.0 ± 0.9	585, 589, 591, 593, 600, 602, 604, 605, 606, 607, 611, 614, 615, 616, 617, 618, 619, 620, 621, 622, 624
V70A	7.4 ± 0.6	589, 590, 596, 600, 602, 604, 605, 606, 607, 610, 612, 615, 616, 617, 618, 620, 624
I44V	13.6 ± 1.2	585, 589, 590, 593, 595, 596, 600, 602, 604, 605, 606, 607, 611, 612, 614, 615, 616, 617, 618, 619, 620, 622, 624
V70I/I44V	39 ± 3.6	588, 591, 596, 600, 606, 622
V70A/I44V	59 ± 1.8	589, 590, 596, 602, 604, 605, 606, 607, 610, 611, 612, 614, 615, 616, 618, 620, 622, 624
I44A	> 1000	
HT6-(GS) ₂ -Ub	11.7 ± 2.1	585, 590, 596, 600, 602, 604, 605, 607, 610, 616, 617, 618, 619, 620, 622, 624
HT6-(GS) ₁₀ -Ub	9.0 ± 1.5	585, 589, 590, 591, 595, 596, 600, 602, 604, 605, 606, 607, 610, 611, 613, 615, 616, 617, 619, 620, 622, 624
M1(1-74)-Ub4	15.6 ± 3.8	585, 596, 600, 602, 604, 606, 607, 615, 616, 617, 618, 620, 622, 624

Table S2. Structural parameters of HT6-Ub and M1 series from SAXS data analysis. Indicated in parentheses are the methods/software used for R_g analysis. ^a R_g and errors were determined from the linear fit of $\ln(I(q))$ vs. q^2 and ^b R_g and errors were determined from choosing multiple values of D_{max} . Data collected in 20 mM sodium phosphate buffer pH 6.8 with 0.5 mM EDTA and 0.02 % NaN_3 .

Construct	R_g (Å) ^a (Guinier) ^a	R_g (Å) ^b (GNOM) ^b	D_{max} (Å) (GNOM)
HT6-(GS)-Ub	37.10 ± 0.06	38.19 ± 0.09	140
HT6-(GS) ₂ -Ub	36.75 ± 0.17	38.08 ± 0.19	137
HT6-(GS) ₄ -Ub	37.65 ± 0.07	38.89 ± 0.10	143
HT6-(GS) ₁₀ -Ub	39.74 ± 0.12	41.37 ± 0.14	148
HT6-(GS) ₂₅ -Ub	47.02 ± 0.62	51.01 ± 0.66	193
HT6-(GS) ₅₀ -Ub	56.31 ± 0.09	58.70 ± 0.15	227
HT6-(PA)-Ub	36.98 ± 0.09	38.12 ± 0.08	129
HT6-(PA) ₂ -Ub	38.03 ± 0.24	39.88 ± 0.26	150
HT6-(PA) ₄ -Ub	40.80 ± 0.06	42.00 ± 0.06	144
HT6-(PA) ₁₀ -Ub	50.52 ± 0.13	52.29 ± 0.20	184
HT6-(PA) ₂₅ -Ub	62.61 ± 0.23	66.24 ± 0.36	249
M1(1-72)	32.03 ± 0.11	34.09 ± 0.15	125
M1(1-73)	33.09 ± 0.07	35.08 ± 0.12	128
M1(1-74)	32.21 ± 0.09	33.76 ± 0.11	122
M1(1-76)	32.42 ± 0.03	34.22 ± 0.21	140
M1(1-76)-PS(GS) ₄	34.04 ± 0.10	35.73 ± 0.17	139
M1(1-74)-A(EA ₃ K) ₃ A	42.06 ± 0.19	45.25 ± 0.40	182
M1(1-74)-A(EA ₃ K) ₆ A	51.84 ± 1.18	56.19 ± 1.42	212
HT6-(GS)-Ub, 200 mM NaCl	36.16 ± 0.18	37.75 ± 0.12	126
HT6-(GS) ₄ -Ub, 200 mM NaCl	37.77 ± 0.14	38.73 ± 0.14	128
HT6-(GS) ₁₀ -Ub, 200 mM NaCl	41.16 ± 0.13	42.32 ± 0.14	142
HT6-(PA)-Ub, 200 mM NaCl	36.85 ± 0.12	37.81 ± 0.14	124
HT6-(PA) ₄ -Ub, 200 mM NaCl	41.05 ± 0.26	42.67 ± 0.24	147
HT6-(PA) ₁₀ -Ub, 200 mM NaCl	50.78 ± 0.16	52.81 ± 0.21	190

Table S3. Inclusion energy values for 450C UBQLN2 & FL UBQLN2 with polyUb ligands (related to Figure 4I, 4J).

Ligand	Inclusion energy (kT)	
	450C UBQLN2	FL UBQLN2
HT6-(GS)-Ub	9.43	-
HT6-(GS) ₂ -Ub	9.83	-
HT6-(GS) ₄ -Ub	10.07	6.67
HT6-(GS) ₁₀ -Ub	10.78	7.07
HT6-(GS) ₂₅ -Ub	11.47	7.79
HT6-(GS) ₅₀ -Ub	13.24	8.80
HT6-(PA)-Ub	9.65	-
HT6-(PA) ₂ -Ub	9.73	-
HT6-(PA) ₄ -Ub	10.16	6.89
HT6-(PA) ₁₀ -Ub	11.35	7.58
HT6-(PA) ₂₅ -Ub	14.13	11.84
M1(1-73)	10.89	-
M1(1-74)	9.78	-
M1(1-76)	10.01	7.62
M1(1-76)-PS(GS) ₄	9.81	-
M1(1-74)-A(EA ₃ K) ₃ A	10.52	7.58
M1(1-74)-A(EA ₃ K) ₆ A	11.15	8.08
K48-Ub ₄	-	14.52
K63-Ub ₄	-	8.42

Table S4. Constructs used in the study

Construct	Sequence
HT6-G ₁₀ -Ub	MTLREIEELLRKIIEDSVRSVAELEDIEKWLKKIGGGGGGGGGG MQIFVKTLTGKTITLEVEPSDTIENVKAKIQDKEGIPPDQQLIFAGKQLEDGRTLSDYNIQ KESTLHLVLRRLGG
HT6-G ₁₀ -Ub V70I	MTLREIEELLRKIIEDSVRSVAELEDIEKWLKKIGGGGGGGGGGMQIFVKTLTGKTITLEV EPSDTIENVKAKIQDKEGIPPDQQLIFAGKQLEDGRTLSDYNIQKESTLHLVLRRLGG
HT6-G ₁₀ -Ub V70A	MTLREIEELLRKIIEDSVRSVAELEDIEKWLKKIGGGGGGGGGG MQIFVKTLTGKTITLEVEPSDTIENVKAKIQDKEGIPPDQQLIFAGKQLEDGRTLSDYNIQ KESTLHLVLRRLGG
HT6-G ₁₀ -Ub I44V	MTLREIEELLRKIIEDSVRSVAELEDIEKWLKKIGGGGGGGGGGMQIFVKTLTGKTITLEV EPSDTIENVKAKIQDKEGIPPDQQLVFAGKQLEDGRTLSDYNIQKESTLHLVLRRLGG
HT6-G ₁₀ -Ub I44A	MTLREIEELLRKIIEDSVRSVAELEDIEKWLKKIGGGGGGGGGGMQIFVKTLTGKTITLEV EPSDTIENVKAKIQDKEGIPPDQQLAFAGKQLEDGRTLSDYNIQKESTLHLVLRRLGG
HT6-G ₁₀ -Ub V70I/I44V	MTLREIEELLRKIIEDSVRSVAELEDIEKWLKKIGGGGGGGGGGMQIFVKTLTGKTITLEV EPSDTIENVKAKIQDKEGIPPDQQLVFAGKQLEDGRTLSDYNIQKESTLHLVLRRLGG
HT6-G ₁₀ -Ub V70A/I44V	MTLREIEELLRKIIEDSVRSVAELEDIEKWLKKIGGGGGGGGGGMQIFVKTLTGKTITLEV EPSDTIENVKAKIQDKEGIPPDQQLVFAGKQLEDGRTLSDYNIQKESTLHLVLRRLGG
HT6-GS-Ub	MTLREIEELLRKIIEDSVRSVAELEDIEKWLKKIGSMQIFVKTLTGKTITLEVEPSDTIENVK AKIQDKEGIPPDQQLIFAGKQLEDGRTLSDYNIQKESTLHLVLRRLGG
HT6-(GS) ₂ -Ub	MTLREIEELLRKIIEDSVRSVAELEDIEKWLKKIGSGSMQIFVKTLTGKTITLEVEPSDTIEN VKAKIQDKEGIPPDQQLIFAGKQLEDGRTLSDYNIQKESTLHLVLRRLGG
HT6-(GS) ₄ -Ub	MTLREIEELLRKIIEDSVRSVAELEDIEKWLKKIGSGSGSMQIFVKTLTGKTITLEVEPS DTIENVKAKIQDKEGIPPDQQLIFAGKQLEDGRTLSDYNIQKESTLHLVLRRLGG
HT6-(GS) ₁₀ -Ub	MTLREIEELLRKIIEDSVRSVAELEDIEKWLKKIGSGSGSGSGSGSGSGSMQIFVK TLTGKTITLEVEPSDTIENVKAKIQDKEGIPPDQQLIFAGKQLEDGRTLSDYNIQKESTLH LVLRRLGG
HT6-(GS) ₂₅ -Ub	MTLREIEELLRKIIEDSVRSVAELEDIEKWLKKIGSGSGSGSGSGSGSGSGSGSGSG SGSGSGSGSGSGSGSGSGSGSMQIFVKTLTGKTITLEVEPSDTIENVKAKIQDKE GIPPDQQLIFAGKQLEDGRTLSDYNIQKESTLHLVLRRLGG
HT6-(GS) ₅₀ -Ub	MTLREIEELLRKIIEDSVRSVAELEDIEKWLKKIGSGSGSGSGSGSGSGSGSGSGSG SGSGSGSGSGSGSGSGSGSGSGSGSGSGSGSGSGSGSGSGSGSGSGSGSGSGSGSG SGSGSGSGSGSGSGSMQIFVKTLTGKTITLEVEPSDTIENVKAKIQDKEGIPPD QQLIFAGKQLEDGRTLSDYNIQKESTLHLVLRRLGG
HT6-PA-Ub	MTLREIEELLRKIIEDSVRSVAELEDIEKWLKKIPAMQIFVKTLTGKTITLEVEPSDTIENVK AKIQDKEGIPPDQQLIFAGKQLEDGRTLSDYNIQKESTLHLVLRRLGG
HT6-(PA) ₂ -Ub	MTLREIEELLRKIIEDSVRSVAELEDIEKWLKKIPAPAMQIFVKTLTGKTITLEVEPSDTIEN VKAKIQDKEGIPPDQQLIFAGKQLEDGRTLSDYNIQKESTLHLVLRRLGG

HT6-(PA) ₄ -Ub	MTLREIEELLRKIIEDSVRSVAELEDIEKWLKIPAPAPAPAMQIFVKTLTGKTITLEVEPSD TIENVKAKIQDKEGIPPDQQLIFAGKQLEDGRTLSDYNIQKESTLHLVLRRLRGG
HT6-(PA) ₁₀ -Ub	MTLREIEELLRKIIEDSVRSVAELEDIEKWLKIPAPAPAPAPAPAPAPAPAPAMQIFVKTL TGKTITLEVEPSDTIENVKAKIQDKEGIPPDQQLIFAGKQLEDGRTLSDYNIQKESTLHLV LRLRGG
HT6-(PA) ₂₅ -Ub	MTLREIEELLRKIIEDSVRSVAELEDIEKWLKIPAPAPAPAPAPAPAPAPAPAPAPAPA PAPAPAPAPAPAPAPAPAPAPAMQIFVKTLTGKTITLEVEPSDTIENVKAKIQDKEGIPPD QQLIFAGKQLEDGRTLSDYNIQKESTLHLVLRRLRGG
M1-Ub4 (1-72)	MQIFVKTLTGKTITLEVEPSDTIENVKAKIQDKEGIPPDQQLIFAGKQLEDGRTLSDYNIQK ESTLHLVLRMQIFVKTLTGKTITLEVEPSDTIENVKAKIQDKEGIPPDQQLIFAGKQLEDGR TLSDYNIQKESTLHLVLRMQIFVKTLTGKTITLEVEPSDTIENVKAKIQDKEGIPPDQQLIFA GKQLEDGRTLSDYNIQKESTLHLVLRMQIFVKTLTGKTITLEVEPSDTIENVKAKIQDKEGIP PDQQLIFAGKQLEDGRTLSDYNIQKESTLHLVLRRLRGG
M1-Ub4 (1-73)	MQIFVKTLTGKTITLEVEPSDTIENVKAKIQDKEGIPPDQQLIFAGKQLEDGRTLSDYNIQK ESTLHLVLRMQIFVKTLTGKTITLEVEPSDTIENVKAKIQDKEGIPPDQQLIFAGKQLEDG RTLSDYNIQKESTLHLVLRMQIFVKTLTGKTITLEVEPSDTIENVKAKIQDKEGIPPDQQLI FAGKQLEDGRTLSDYNIQKESTLHLVLRMQIFVKTLTGKTITLEVEPSDTIENVKAKIQDKE GIPPDQQLIFAGKQLEDGRTLSDYNIQKESTLHLVLRRLRGG
M1-Ub4 (1-74)	MQIFVKTLTGKTITLEVEPSDTIENVKAKIQDKEGIPPDQQLIFAGKQLEDGRTLSDYNIQK ESTLHLVLRMQIFVKTLTGKTITLEVEPSDTIENVKAKIQDKEGIPPDQQLIFAGKQLED GRTLSDYNIQKESTLHLVLRMQIFVKTLTGKTITLEVEPSDTIENVKAKIQDKEGIPPDQQ RLIFAGKQLEDGRTLSDYNIQKESTLHLVLRMQIFVKTLTGKTITLEVEPSDTIENVKAKIQ DKEGIPPDQQLIFAGKQLEDGRTLSDYNIQKESTLHLVLRRLRGG
M1-Ub4 (1-76)	MQIFVKTLTGKTITLEVEPSDTIENVKAKIQDKEGIPPDQQLIFAGKQLEDGRTLSDYNIQK ESTLHLVLRRLRGMQIFVKTLTGKTITLEVEPSDTIENVKAKIQDKEGIPPDQQLIFAGKQL EDGRTLSDYNIQKESTLHLVLRRLRGMQIFVKTLTGKTITLEVEPSDTIENVKAKIQDKEGIP PDQQLIFAGKQLEDGRTLSDYNIQKESTLHLVLRRLRGMQIFVKTLTGKTITLEVEPSDTI ENVKAKIQDKEGIPPDQQLIFAGKQLEDGRTLSDYNIQKESTLHLVLRRLRGG
M1(1-76)-PS(GS) ₄ (linker in orange)	MQIFVKTLTGKTITLEVEPSDTIENVKAKIQDKEGIPPDQQLIFAGKQLEDGRTLSDYNIQK ESTLHLVLRRLRGG PSGSGSGSGSMQIFVKTLTGKTITLEVEPSDTIENVKAKIQDKEGIPPD QQLIFAGKQLEDGRTLSDYNIQKESTLHLVLRRLRGG PSGSGSGSGSMQIFVKTLTGKTIT LEVEPSDTIENVKAKIQDKEGIPPDQQLIFAGKQLEDGRTLSDYNIQKESTLHLVLRRLRGG PSGSGSGSGSMQIFVKTLTGKTITLEVEPSDTIENVKAKIQDKEGIPPDQQLIFAGKQLED GRTLSDYNIQKESTLHLVLRRLRGG
M1(1-74)- A(EA ₃ K) ₃ A (linker in orange)	MQIFVKTLTGKTITLEVEPSDTIENVKAKIQDKEGIPPDQQLIFAGKQLEDGRTLSDYNIQK ESTLHLVLRRLR AEAAAKEAAAKEAAAKAMQIFVKTLTGKTITLEVEPSDTIENVKAKIQDKEG IPPDQQLIFAGKQLEDGRTLSDYNIQKESTLHLVLRRLR AEAAAKEAAAKEAAAKAMQIFVK TLTGKTITLEVEPSDTIENVKAKIQDKEGIPPDQQLIFAGKQLEDGRTLSDYNIQKESTLHL VLRRLR AEAAAKEAAAKEAAAKAMQIFVKTLTGKTITLEVEPSDTIENVKAKIQDKEGIPPDQ QLIFAGKQLEDGRTLSDYNIQKESTLHLVLRRLRGG
M1(1-74)- A(EA ₃ K) ₆ A (linker in orange)	MQIFVKTLTGKTITLEVEPSDTIENVKAKIQDKEGIPPDQQLIFAGKQLEDGRTLSDYNIQKE STLHLVLRRLR AEAAAKEAAAKEAAAKEAAAKEAAAKAMQIFVKTLTGKTITLEVEPSD TIENVKAKIQDKEGIPPDQQLIFAGKQLEDGRTLSDYNIQKESTLHLVLRRLR AEAAAKEAAAK EAAAKEAAAKEAAAKEAAAKAMQIFVKTLTGKTITLEVEPSDTIENVKAKIQDKEGIPPDQQL IFAGKQLEDGRTLSDYNIQKESTLHLVLRRLRAEAAAKEAAAKEAAAKEAAAKEAAAKEAAAKA

	MQIFVKLTGTGKTITLEVEPSDTIENVKAKIQDKEGIPPDQQLIFAGKQLEDGRTLSDYNIQKE STLHLVLRRLGG
UBQLN2 450C	MRAMQALMQIQQLQTLATEAPGLIPSFTPGVGVGLGTAIGVGPVTPIGPIGPIVPFTP IGPIGPIGPTGPAAPPSTGSGGPTGPTVSSAAPSETTSPTSESGPNQQFIQMQVQALA GANAPQLPNPEVRFQQQLQLNAMGFLNREANLQALIATGGDINAAIERLLGSQPSW

Table S5. SEC-MALS-SAXS Data Collection and Analysis for all Ub hubs in this study

- See attached Excel file.

Table S6. SASSIE parameters and results for generation of ligand hub conformational ensembles

Ligand hub	Flexible component of starting structure	Structures Generated	Accepted	Best single structure (reduced χ^2)	Number of structures with lowest χ^2
HT6-(PA) ₄ -Ub	35-42, 115-118	30000	20613	2.77	83 $\chi^2 < 4$
HT6-(PA) ₁₀ -Ub	35-54, 126-129	30000	18786	1.06	13 $\chi^2 < 1.5$
M1-Ub ₄ (1-72)	72-73, 144-145, 216-217, 288-292	30000	13449	0.86	44 $\chi^2 < 1.0$
M1-Ub ₄ (1-74)	72-74, 146-148, 220-222, 294-298	30000	18927	1.03	47 $\chi^2 < 1.5$
M1-Ub ₄ (1-74) A(EA ₃ K) ₆ A	72-76, 105-107, 178-182, 211-213, 284-288, 317-319, 390-394	30000	19359	0.63	140 $\chi^2 < 0.75$